J. Phys. Chem. A **1998,** *102,* 8695−8707

Rotational State Resolved Differential Cross Sections for the Reaction $F + D_2 \rightarrow DF + D$ at Collision Energies 140−240 meV

M. Faubel,* B. Martínez−Haya,† L. Y. Rusin,‡ U. Tappe, and J. P. Toennies
Max−Planck−Institut für Strömungsforschung, D-37073 Göttingen, Germany

F. J. Aoiz and L. Bañares
Departamento de Química Física, Facultad de Química, Universidad Complutense, E-28040 Madrid, Spain

Received: June 4, 1998; In Final Form: July 27, 1998

Product rotationally state-resolved differential cross sections (DCS) have been determined for the DF(v_f, j_f) products of the $F + D_2$ ($v_i = 0$, $j_i = 0, 1, 2$) reaction from the detailed analysis of high resolution crossed molecular beam experiments at the collision energies of 140, 180, and 240 meV. An increasing rotational excitation when going from the backward to the sideways and forward scattering regions is observed for all vibrational DF states, except for $v_f = 4$. The DF products in $v_f = 4$ scattered in the forward region ($\theta_{cm} = 0°−20°$) are rotationally cooler than those scattered at intermediate scattering angles ($\theta_{cm} = 30°−100°$). The experimental results are compared with quasiclassical trajectory (QCT) calculations on the ab initio potential energy surface (PES) of Stark and Werner. Good qualitative agreement is found for the observed trend of the v_f, j_f state-resolved DCSs. In particular, the behavior of the $v_f = 4$ product state is well accounted for by the QCT calculation. The results are discussed in terms of the quasiclassical state-to-state reaction probabilities as a function of the total angular momentum (opacity functions).

I. Introduction

The $F + H_2 \rightarrow HF + H$ reaction and its isotopic variants have become a benchmark in the field of reaction dynamics and played a key role in both theoretical and experimental studies of reactive scattering (for a recent review see ref 1 and for work up to 1980 see ref 2). A major breakthrough in the study of this reaction occurred with the molecular beam experiments reported by Lee and co-workers in 1985.[3,4] A series of systematic measurements at different collision energies allowed the authors to extract a very comprehensive picture of the dynamical behavior of the reaction. The resolution achieved in these experiments was unprecedented for the study of any reaction at the time, and remained so for several years. The experimental results, consisting on laboratory (LAB) product angular distributions (AD) and time-of-flight (TOF) spectra, yielded fully vibrationally state-resolved differential cross sections (DCS) at several collision energies for the $F + H_2$ reaction and its isotopic variants, $F + D_2$ and $F + HD$, which were elegantly presented as angle−velocity contour polar maps obtained following the suitable transformation from the LAB to the center-of-mass (CM) frame.

During the last few years, our group in Göttingen has thoroughly investigated the $F + D_2$ isotopic variant of the reaction at several collision energies within the range 82.5−240 meV (1.9−5.5 kcal mol^{-1}).[5−11] In these newer experiments, using a conventional crossed molecular beam machine but with a resolution between 3 to 4 times higher than that of Lee and co-workers, a more accurate evaluation of the vibrationally state-resolved differential and integral reaction cross sections became possible. In particular, careful calibration experiments allowed for the first time the determination of absolute values of the integral and differential reaction cross sections.[5,10] In addition, a strong dependence of the reactive DCSs on the D_2 initial rotational state was observed[6] and inelastic (nonreactive) scattering experiments of the $F + H_2/D_2$ were also performed, mainly to determine the long-range interaction part of the reagents.[12]

From the theoretical side, the advent of a fully ab initio potential energy surface (PES) by Stark and Werner (hereafter SW)[13] has allowed the simulation[14] of the experiments of Lee and co-workers[3] for the $F + H_2$ reaction based on quantum mechanical (QM)[15] and quasiclassical trajectory (QCT) calculations.[16] The simulations[14] using the QM DCSs showed an unprecedentedly good agreement with the experimental LAB ADs and TOF spectra. In particular, the height of the peak in the experimental LAB AD corresponding to the conspicuous HF($v_f = 3$) CM forward scattering was quite well reproduced. The simulations based on QCT data failed to account for most of the $v_f = 3$ forward peak, although sideward and backward scattering was very well accounted for. One of the main conclusions of that work was the importance of performing simulations of the experimental dynamical observables in the LAB system to assess the quality of a given calculation on a given PES.[14] For the $F + D_2$ isotopic variant, simulations based on QCT calculations on the SW PES have shown somewhat better agreement with the experimental results[17,18] than those for the $F + H_2$, but nevertheless, the forward scattering into $v_f = 4$ is also underestimated in the classical calculation. Recent QM calculations on the SW PES at 90 meV[9,19] and at 140 meV collision energies[19] have shown good agreement with the v' state-resolved experimental DCSs.[6,9,10]

---

* Corresponding author.

† Present address: Departamento de Química Física, Facultad de Química, Universidad Complutense, E-28040 Madrid, Spain.

‡ Institute of Energy Problems of Chemical Physics, Leninskii prospect 38, Bldg. 2, Moscow 117829, Russia.

10.1021/jp982488k CCC: $15.00

TABLE 1: Experimental Conditions of the F atom (10% F_2/Ar mixture) and the Converted Molecular D_2 (90% ortho−D_2, 10% para−D_2) Supersonic Beams: Average Beam Velocities, v_F, v_{D_2}, and Collision energy, E_{cm}, Rotational Temperature of the D_2 Beam T_{rot}, and Rotational Populations $\rho(j_i)$

					$\rho(j_i)$			
experiment[a]	E_{cm} [meV]	v_F [m/s]	v_{D_2} [m/s]	T_{rot} [K]	$j_i = 0$	$j_i = 1$	$j_i = 2$	$j_i \geq 3$
C_1, C_2	140 ± 3	1130 ± 35	2620 ± 40	60	0.85	0.10	0.05	0.00
D_1	180 ± 3	1125 ± 35	3020 ± 45	85	0.74	0.10	0.16	0.00
D_2	180 ± 3	1160 ± 35	3020 ± 45	85	0.74	0.10	0.16	0.00
E_1	240 ± 5	1165 ± 35	3530 ± 55	115	0.59	0.09	0.31	0.01
E_2	239 ± 5	1165 ± 35	3530 ± 55	135	0.52	0.09	0.37	0.02
E_3	241 ± 6	1150 ± 45	3560 ± 80	175	0.41	0.08	0.47	0.04

[a] Notation as in ref 10.

The original experiments of Lee and co-workers had not enough resolution, however, to yield information about rovibrational state-resolved DCSs. The availability of experimental v_f, j_f integral and differential cross sections could provide a better means for the assessment of the ab initio PESs and the different dynamical calculations. Recently, a considerable amount of experimental effort has gone into measuring v_f, j_f resolved integral and differential cross sections for this reactive system. In this direction, Chapman et al.[20] have reported the measurement of the nascent rotational HF($v_f = 3$, j_f) distribution for the F + H_2 reaction using crossed molecular beams and infrared (IR) direct absorption of the products at a collision energy of 1.8 kcal mol^{-1}. The experimental integral cross sections were compared with QM calculations carried out on the SW PES at 1.84 kcal mol^{-1} by Castillo and Manolopoulos.[15] The most important conclusion was that the experimental rotational distribution into $v_f = 3$ is hotter than the theoretical one, and that HF($v_f = 3$, j_f) product channels, which are energetically closed to reaction in the QM calculations on the SW PES, were found to be experimentally accessible at that collision energy. One possible explanation for the observed discrepancies can be the contribution to reaction from nonadiabatic channels involving F($^2P_{1/2}$) atoms which are also present in the atomic beam.

Keil and co-workers[21,22] have carried out new crossed molecular beam experiments also for the F + H_2 reaction. Angular distributions were measured for individual v_f, j_f state-resolved states of HF by using IR laser excitation and bolometric detection of the products. The technique is sensitive to population differences between $v_f = 1$, j_f and $v_f = 2$, $j_f - 1$ HF states as a function of the LAB scattering angle. The measured LAB ADs were reproduced very well by simulations using QM v_f, j_f state-resolved DCSs calculated on the SW PES by Castillo and Manolopoulos[15] at a slightly different collision energy. A very interesting finding was the presence of HF($v_f = 1$, j_f) scattering in the forward hemisphere in the CM frame, which was well accounted for by simulations using the QM state-resolved DCSs of Castillo and Manolopoulos. Since the QCT results of Aoiz et al.[16] on the same surface did not show appreciable scattering in the forward hemisphere for HF($v_f = 1$), this feature was attributed to a quantum mechanical effect.[21,22] However, recent simulations based on new, better converged, QM calculations on the SW PES at exactly the same collision energy have not been able to reproduce this feature.[23]

Although no separated v_f, j_f peaks have been resolved in the TOF spectra measurements carried out in the experiments of Göttingen for the F + D_2 reaction, at 90 meV collision energy a careful analysis of the envelopes has allowed the extraction of v_f, j_f state-resolved DCSs in the CM frame.[11] The results reveal that the backward scattered DF($v_f = 2-3$) products show a bimodal structure of their rotational distribution. This bimodality has been well reproduced by QM calculations performed on the SW PES.[11,19]

In the present work, we report on rovibrationally state-resolved DCSs for the F + D_2 reaction at the collision energies of 140, 180, and 240 meV (3.23, 4.15, and 5.53 kcal mol^{-1}) from high resolution crossed molecular beam experiments. The experimentally evaluated v_f, j_f CM DCSs are extensively compared with the results of QCT calculations for the title reaction performed on the SW PES at exactly the same experimental conditions.

The paper is organized as follows: section II describes the experimental setup and the method of analysis used to evaluate the v_f, j_f CM DCSs from the measured TOF spectra. In section III, the QCT method employed for the dynamical calculations is briefly reviewed. Section IV contains selected experimental TOF spectra and experimental v_f, j_f state-resolved DCSs and their comparison with the QCT results. The discussion is presented in section V, and finally, the conclusions are summarized in section VI.

II. Experimental Section

A. Apparatus and Time−of−Flight Spectra. The crossed molecular beam scattering apparatus used in the present experiments has been described in detail elsewhere,[5] and only some general features are discussed here. The argon-seeded F atom and the D_2 reactant beams are produced in supersonic expansions involving large fluxes and high speed ratios. Atomic fluorine is produced by thermal dissociation of molecular fluorine in a 10% mixture in argon in a homemade magnesium fluoride oven[24] at temperatures ranging 1100−1220 K. Both beams pass through three differential pumping stages before entering the scattering chamber where the background pressure is kept below 10^{-7} torr. The DF reaction products travel then over a flight path of about 146 cm through four additional differential pumping stages before reaching an electron bombardment ionizer followed by a magnetic mass spectrometer and an electron multiplier.

The state-to-state DCSs obtained in the present work were determined from a series of crossed beam experiments at three different average collision energies: 140 ± 3 meV (3.23 kcal mol^{-1}), 180 ± 4 meV (4.15 kcal mol^{-1}), and 240 ± 5 meV (5.53 kcal mol^{-1}). Table 1 lists some of the relevant experimental parameters of the F atom (10% F_2/Ar mixture) and the converted molecular D_2 (90% ortho-D_2, 10% para-D_2) supersonic beams in each of the experiments, namely, the average beam velocities v_F and v_{D_2}, the rotational temperature of the D_2 beam, T_{rot}, and the corresponding rotational populations, $\rho(j_i)$. A complete characterization of the experimental conditions for the reactant beams, the stagnation pressure and temperature, the nozzle orifice, gas flow, etc., can be found in refs 6 and 10 (140 meV) and refs 8 and 10 (180 and 240 meV). In those

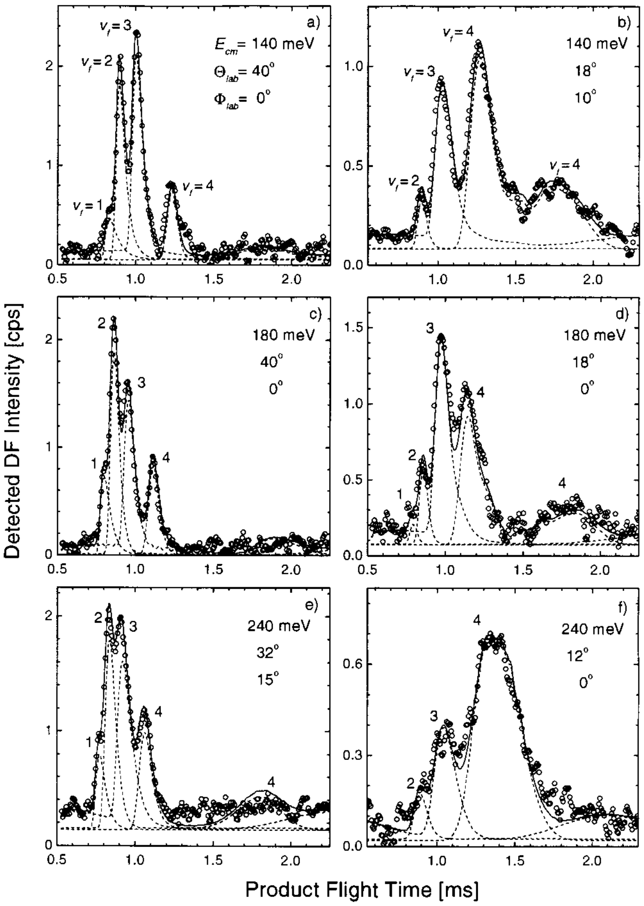

Figure 1. Typical TOF spectra (open circles) of the DF products at the collision energies: (a) and (b) 140 meV, (c) and (d) 180 meV, (e) and (f) 240 meV. Θ_{lab} and Φ_{lab} denote the in-plane and out-of-plane LAB scattering angles, respectively (see text). The product vibrational state v_f associated to each peak in the spectra is indicated. The best fit simulations to the TOF spectra are shown with lines.

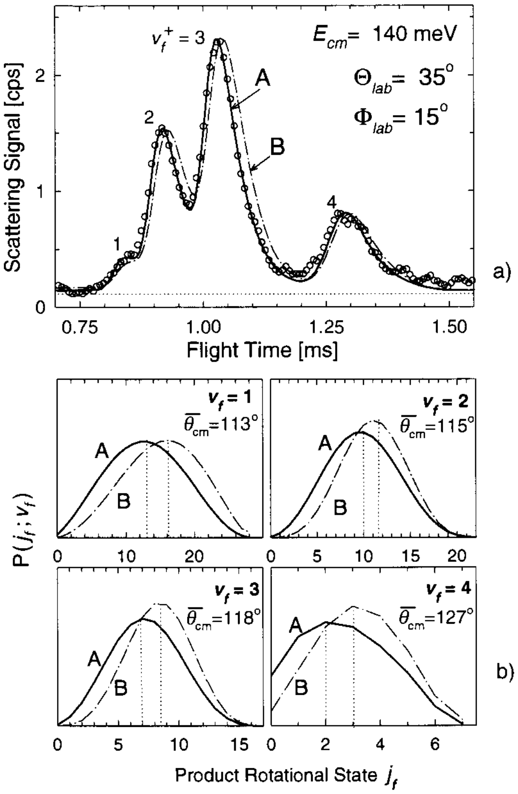

Figure 2. a) Trial simulations for a typical TOF spectra at 140 meV collision energy with the different DF product rotational distributions $P(j_f;v_f = 1-4)$ (eq 2) shown in b). At the LAB angles $\Theta_{lab} = 35°$, $\Phi_{lab} = 15°$, the detected DF products are scattered in the interval $\theta_{cm} \approx 110-130°$ in the CM frame. The average CM scattering angle $\bar{\theta}_{cm}$, spanned for the j_f states within each v_f envelope is indicated. The best fit simulation A was calculated with the $P(j_f;v_f)$ distributions also denoted A in the lower parts. The simulation B was obtained with the distributions denoted B in the lower parts which are displaced by between one to three rotational quanta with respect to the best fit ones A.

previous reports,[6,8,10] the experiments were described in detail and were analyzed for vibration state distributions only. The vibrationally state-resolved DCSs in absolute units were then presented, while here we consider the rotational envelopes of the vibrational time-of-flight peaks.

Typically, between 20 and 30 TOF spectra of the DF products were measured at each collision energy covering the appropiate set of LAB angles Θ_{lab} (in the plane of the incident beams, with respect to the direction of the incoming F atom beam) and Φ_{lab} (perpendicular plane angle),[5] in order to span the relevant CM scattering angles, θ_{cm}. Figures 1−3 show just a small selection of the measured TOF spectra. A larger selection of TOF spectra can be found in refs 6, 8, and 25. The optimal set of LAB angles within the hemispherical scattering region accessible to the detector was chosen at each collision energy in order to study the different CM angles with the best possible energy resolution, for which scattering angles out of the collision plane ($\Phi_{lab} > 0°$) are often favorable.[5,25] The product energy resolution (full width at half-maximum, fwhm) achieved in the spectra is angle and state dependent and ranges from 20−40 meV for $v_f = 4$, the highest vibrational state accessible, to 100−200 meV for $v_f = 1$, the lowest observed vibrational state.[5,25] This is more than a factor of three greater than the resolution achieved in previous crossed beam experiments employing similar detection techniques[3] and allows for a more precise evaluation of the state-resolved DCSs.

B. Evaluation of Rotationally State-Resolved Differential Cross Sections. The method followed for the evaluation of v_f, j_f state-resolved DCSs from the measured TOF spectra has been discussed in detail in previous works.[8,10] The analysis of the time-dependent scattering intensity in the complete set of TOF measurements is perfomed simultaneously by deconvoluting a trial set of v_f, j_f CM DCSs by means of a three-dimensional Monte Carlo sampling of the velocity and spatial density distributions of the F and D_2 reagent beams and of the angular acceptance of the detector (eq 1 of ref 8).

The numerical convolution was averaged over the initial rotational states of D_2, $j_i = 0$, 1 and 2, with weights corresponding to the experimental estimated relative populations.[8,10] All the experiments discussed in the present paper were performed with a cryogenically catalyzed mixture of 90% ortho-deuterium and 10% para-deuterium with estimated rotational temperatures for the D_2 molecules in the reactant beam of 60, 85, and 115−175 K for the experiments at 140, 180, and 240 meV, respectively.[10,25] The corresponding j_i populations are listed in Table 1.

As in our previous works, only F atoms in the $^2P_{3/2}$ ground state were assumed to take part in the reaction. At a typical fluorine source operating temperature of 1150 K, about 23% of the F atoms are estimated to be in the $^2P_{1/2}$ excited fine-structure electronic state, which lies ~50 meV above the ground state. Some evidence for the $F(^2P_{1/2}) + D_2$ reaction with a cross section at least 1 order of magnitude smaller than that for the ground state $F(^2P_{3/2}) + D_2$ reaction has been recently reported.[5,7] In view of this small reaction cross section, and since all the

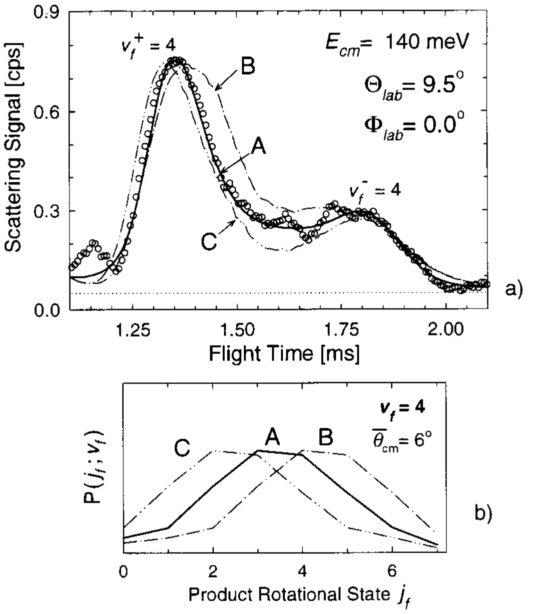

Figure 3. Same as Figure 3 but for a TOF spectrum at 140 meV collision energy and $\Theta_{lab} = 9.5°$, $\Phi_{lab} = 0°$. Here, DF($v_f = 4$) products scattered at $\theta_{cm} \approx 0°-15°$ are detected. In this case the simulations B and C have been calculated after displacing the product state distributions P(j_f;v_f) by one rotational quantum number with respect to the best fit distribution A.

TOF spectra in the present work could be correctly fitted without any reactive contribution from F($^2P_{1/2}$) atoms, this channel was ignored in the present analysis.

The DCSs for each product vibrational and rotational state were constructed according to the expression[8]

$$\frac{d\sigma}{d\omega}(v_f, j_f;\theta_{cm}) = A(v_f, \theta_{cm})P(j_f;\, v_f, \theta_{cm}) \qquad (1)$$

where A (v_f, θ_{cm}) defines the v_f DCS summed on j_f at the CM scattering angle θ_{cm} and P (j_f; v_f,θ_{cm}) is a normalized rotational distribution. Throughout the present discussion, the CM scattering angle $\theta_{cm} = 0°$ corresponds to a DF product velocity in the direction of the initial F atom CM velocity (forward scattering).

Absolute values for the v_f state-resolved DCSs (i.e., for the $A(v_f,\theta_{cm})$ values) were obtained by means of a careful calibration of the beam intensities and product detection efficiency[10] with the aid of additional nonreactive scattering experiments on the Ar$-$D$_2$ system, whose interaction is well characterized.[26] The absolute calibration of the F$-$D$_2$ reactive experiment is then basically determined by two *relative* magnitudes: the ratio between the density of Ar atoms and reactive F atoms in the scattering center, and the ratio of detection efficiencies for DF molecules versus Ar atoms. Whereas the former quantity could be measured in situ during the experiment, the latter was estimated from available theoretical data. The whole procedure is discussed in detail in previous publications.[5,10,24,25] The uncertainty in the absolute value of the state-to-state reaction cross sections evaluated from the present experiments is estimated to be 50%. The uncertainty in the determination of relative v_f state-resolved cross sections, (i.e., the relative ratio between the total DCS of two different vibrational states at arbitrary scattering angles, is much less, typically 10%. The uncertainty attained in the relative values of the v_f, j_f state-resolved DCSs is somewhat larger, typically 20%, as discussed below in this section.

The rotational distribution $P(j_f;v_f,\theta_{cm})$ was chosen to be function of two angle-dependent fit parameters, $\alpha(v_f,\theta_{cm})$ and $E(v_f,\theta_{cm})$, which determine, respectively, the maximum and the width of the distribution[8,25]

$$P(j_f;v_f,\theta_{cm}) = N\int_{j_f+1}^{j_f} dj\,(j + {}^1/_2)\left(\frac{E_{rot}(j)}{E_{rec}(v_f)}\right)^{\alpha(v_f,\theta_{cm})}\left(1 - \frac{E_{rot}(j)}{E_{rec}(v_f)}\right)^{\beta(v_f,\theta_{cm})} \qquad (2)$$

where $\beta(v_f,\ \theta_{cm})$ is given by

$$\beta(v_f,\ \theta_{cm}) = \alpha(v_f,\ \theta_{cm})\left(\frac{E(v_f,\ \theta_{cm})}{1 - E(v_f,\ \theta_{cm})}\right)$$

In eq 2, $E_{rec}(v_f,\ \theta_{cm}) = \Delta D_0 + E_{cm} - E_{vib}$ is the maximum recoil energy of the vibrational state v_f, with ΔD_0 being the reaction exothermicity, E_{cm} the collision energy and E_{vib} and E_{rot}, the product state vibrational and rotational energies. N is a normalization constant.

In the early scattering studies of the F + D$_2$ reaction from our group,[5] Boltzmann-like product rotational distributions were assumed to analyze the TOF spectra with an effective temperature as the only fit parameter. However, significant deviations from the Boltzmann j_f dependence were observed in more recent experiments at collision energies between 90$-$240 meV.[6-8] Therefore, we introduced the two-parameter functional P (j_f;v_f,θ_{cm}) described in eq 2, which is consistent with that previously suggested by Neumark et al.,[3] and provides satisfactory fits to our TOF measurements at all scattering angles and collision energies investigated.

High resolution experiments have allowed recently the observation of bimodal rotational distributions for DF($v_f = 2$, 3) product at 90 and 110 meV collision energies.[11,25] The double-peaked j_f distributions were modeled by replacing eq 2 with a four-parameter expression involving two independent distributions (eq 2 in ref 11). In the experiments considered here at 140$-$240 meV collision energies, however, no evidence of bimodal distributions was found, and the envelope of the v_f peaks in all TOF spectra could be correctly evaluated using the two-parameter (monomodal) form given in eq 2.

Angle$-$velocity contour polar maps have been derived from the fully v_f, j_f state-resolved DCSs after including the broadening given by the product energy resolution achieved in the present experiments. The final expression for the CM angle$-$velocity distribution is given by[16]

$$P(w,\ \theta) = \sum_{j=0}^{2}\rho(j)\sum_k N_k \exp\left[-\left(\frac{w - w_k}{\Delta w_k}\right)^2\right]\left(\frac{d^2\sigma}{d^2\omega}\right)_k \qquad (3)$$

where the sum in $k \equiv (v_f,\ j_f)$ extends to all final rovibrational states of the products which are energetically accessible, and the sum in j_i considers the initial D$_2$ rotation with $\rho(j)$ denoting the relative population of the j_i = 0, 1, 2 states (Table 1). The experimental uncertainty in the CM recoil velocity w is modeled with a Gaussian distribution centered in every case at w_k, the recoil velocity associated with the internal state k, and with a width Δw_k. The N_k are the normalization constants of the Gaussian profiles. The fwhm, given by $2\sqrt{\ln 2}\Delta w_k/w_k$, was 7% in all cases, which corresponds to 14% of uncertainty in the CM energy of the DF product.

The best fit simulations to the TOF measurements in Figures 1$-$3 are shown in the same figures as solid lines. As can be seen, a very good agreement is found between the best-fit simulated and the measured spectra, the location and shape of the observed vibrational TOF peaks being well reproduced in all cases. Although the resolution of the TOF spectra does not allow for the observation of individual rotational states of the DF products, it is shown below that the shape of the rotational envelope within each final vibrational TOF peak provides sensitive information on the j_f distribution of the DF product molecules.

The sensitivity of the present measurements to changes in the best-fit v_f, j_f state-resolved DCSs is exemplified in Figures 2 and 3 for two of the TOF spectra measured at 140 meV collision energy. In this case, the product energy resolution is typically 150, 100, 50, and 25 meV for the product states $v_f = 1, 2, 3$, and 4, respectively. The j_f distributions associated with the different trial fits of the spectra in Figures 2 and 3 are meant for illustration purposes only and are averaged over the θ_{cm} interval spanned for each v_f, j_f state at the given LAB scattering angles.

Figure 2 displays the result of the analysis of a typical TOF measurement at $\Theta_{lab} = 35°$, $\Phi_{lab} = 15°$ which covers the reactive scattering into the CM sideways region ($\theta_{cm} \simeq 110°-130°$, depending on the final vibrational state, $v_f = 1-4$). The result of the best-fit simulation to the measurement (denoted by "A") is shown together with a trial simulation ("B") in which the maxima of the product final rotational distributions have been shifted toward larger j_f values (by one rotational quantum number for $v_f = 4$, by roughly one and a half for $v_f = 3$ and 2 and by three rotational quantum numbers for $v_f = 1$) as displayed in the lower parts of Figure 2. Such changes account for shifts in the maxima of the product translational energy distribution by $\Delta E_T = 115$, 40, 20, and 7 meV for $v_f = 1, 2, 3$, and 4, respectively, and are clearly observable in the experiment. In fact, the comparison of simulations A and B in Figure 2 shows that the TOF measurement is actually sensitive to smaller changes in the trial $P(j_f;v_f)$ distribution than those proposed in the example, especially for $v_f = 2$ and 3. Notice also that for $v_f = 4$, the best experimentally resolved vibrational product, the relatively small displacement by only 7 meV of the maximum of the product rotational energy distribution (from $j_f = 2$ to $j_f = 3$) results already in a detectable displacement of the simulated TOF peak toward longer flight times with respect to the measured peak.

In Figure 3 a similar analysis is carried out for a TOF spectrum at $\Theta_{lab} = 9.5°$, $\Phi_{lab} = 0°$. This is a typical measurement at 140 meV in the forward scattering region ($\theta_{cm} < 15°$) of DF($v_f = 4$). The faster and narrower peak of the two observed in the TOF spectrum (denoted $v_f^+ = 4$ in Figure 3) originates from CM scattering angles strictly smaller than 15°, whereas for the slower and broader peak (denoted $v_f^- = 4$) somewhat larger CM scattering angles are involved (10°−35°). Two trial simulations (B and C) are compared with the best fit simulation (A) and with the experimental TOF spectrum in Figure 3, in order to investigate the effect induced by a shift of the trial j_f distribution by (plus or minus) one quantum number. As can be seen, significant differences are apparent between the different simulated spectra in spite of the relatively small change in the product translational energy introduced by the displaced trial j_f distributions. Note that the internal energy of the DF states with maximum cross section in the cases B, $v_f = 4$, $j_f = 4$; and C, $v_f = 4$, $j_f = 2$; differs by only ~17 meV. The rotational distribution B, displaced by one quantum number toward larger j_f values with respect to the best-fit distribution, leads to a $v_f^+ = 4$ TOF peak which is noticeably slower and broader than the measured one. On the other hand, the rotationally cooler trial j_f distribution C yields a simulated peak which is appreciably faster than the experimental one. The fact that the analysis is more sensitive to displacements of the best fit distribution toward larger j_f states (B) than toward smaller ones (C) is due to the larger change in the rotational energy involved, and is additionally reinforced by the larger Jacobi factors $|d\omega/d\Omega|$ in the CM−LAB transformation for the higher rotational states of $v_f = 4$.

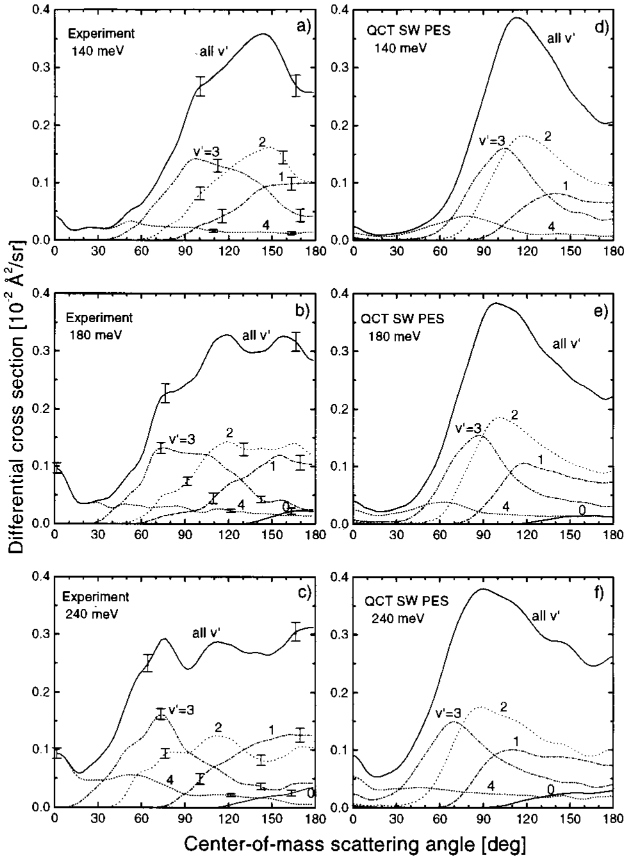

Figure 4. Center-of-mass differential cross sections for the DF product molecules in the vibrational states $v_f = 0-4$ from the F + D_2 reaction at collision energies of 140, 180, and 240 meV: (a−c) experiment; (d−f) QCT calculation on the SW PES. The error bars indicate the experimental uncertainty in the determination of the relative value of the DCS of two arbitrary vibrational states at representative scattering angles. Note that the experimental cross sections are given in absolute units of Å^2/sr (with an uncertainty of 50%; see text and ref 10).

From the results presented in Figures 2 and 3, it can be concluded that the energy resolution achieved in the present experiments is sufficient to evaluate the location of the maximum and the width of the rotational distribution of the DF(v_f) products with an uncertainty Δj of one rotational quantum for $v_f = 3$ and 4, of two quanta for $v_f = 2$, and of three to four quanta for $v_f = 1$. In relative terms, the rotational distributions $P(v_f,j_f)$ of the best resolved vibrational states, $v_f = 3$ and $v_f = 4$, are evaluated in the present experiments within an accuracy of typically 20%.

III. Quasiclassical Trajectory Method

The general method of calculation of quasiclassical trajectories is the same one as used in previous works. It is described more extensively in refs 18 and 27, and only the particular details relevant to the present work are given here.

The calculations have been performed on the ab initio SW PES for the F + D_2 ($v_i = 0$, $j_i = 0, 1, 2$) reaction at the collision energies of 140, 180, and 240 meV, corresponding to the average

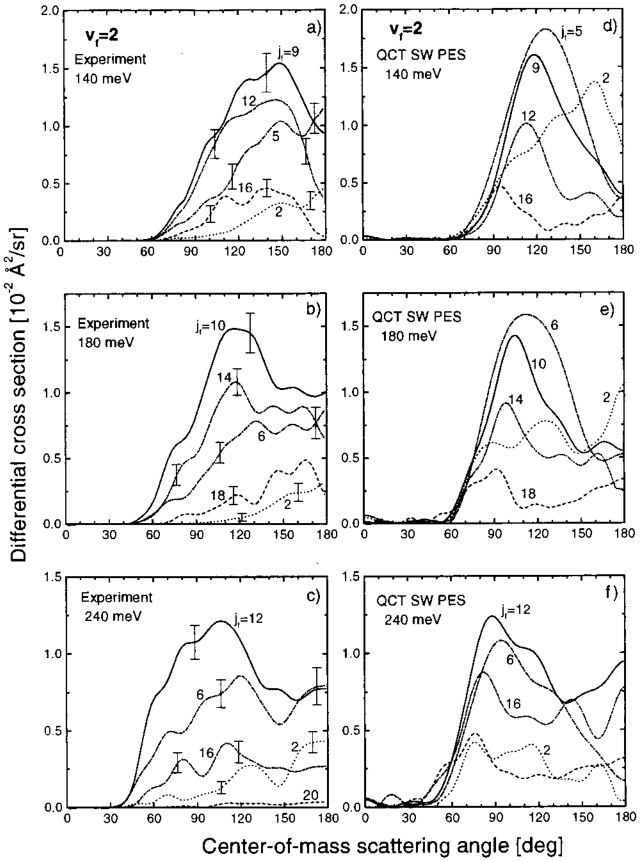

Figure 5. Selected center-of-mass differential cross sections for the DF($v_f = 2$, j_f) product molecules in representative rotational states j_f from the F + D_2 reaction at the collision energies of 140, 180, and 240: (a−c) Experiment; (d−f) QCT calculation on the SW PES. The uncertainty attained in the experimental relative values of the v_f, j_f state-resolved DCSs is illustrated with the error bars. Note that the experimental cross sections are given in absolute units of Å²/sr (with an uncertainty of 50%; see text and ref 10).

collision energies of the molecular beam experiments discussed above. Batches of 60 000 trajectories have been calculated at each energy and initial rotational quantum number j_i.

As in a previous study,[18] the quantization of the rotational angular momentum of the D_2 reagent and of the DF product was performed semiclassically by equating the square of the rotational angular momentum to $(j_i + {}^1/_2)^2\hbar^2$ (Langer correction). With the (real) j_f value so obtained for the DF products, the vibrational quantum number v_f was found by equating the internal energy of the outgoing molecule to a rovibrational Dunham expansion containing 20 terms (fourth power in $v_f + {}^1/_2$ and third power in $(j_f + {}^1/_2)^2$) calculated by fitting the rovibrational energies given by the asymptotic diatomic limits of the SW PES. The values of v_f and j_f found in this way were then rounded to the nearest integer.

The vibrationally and rotationally state-resolved DCSs were calculated by the method of moments expansion in Legendre polynomials.[18,27] The truncation of the series is addressed by performing the Smirnov−Kolmogorov test of the cumulative probability distribution. Significance levels higher than 95% were achieved using 8−12 Legendre moments, ensuring a very good convergence. Angle−velocity contour polar maps including the experimental broadening were calculated from the v_f, j_f state-resolved DCSs as described in section II.B. The simulation of the TOF spectra using the QCT CM DCSs was carried out by means of the same Monte Carlo procedure employed for the evaluation of the experimental DCSs.[8,28] All the simulations of the LAB and CM experimental results for the F + D_2 reaction were made by appropriately weighting on the initial rotational quantum number j_i of the D_2 reagent (Table 1). It should be stressed that, since the experimental DCSs are absolutely calibrated, the QCT simulations do not contain any adjustable parameter.

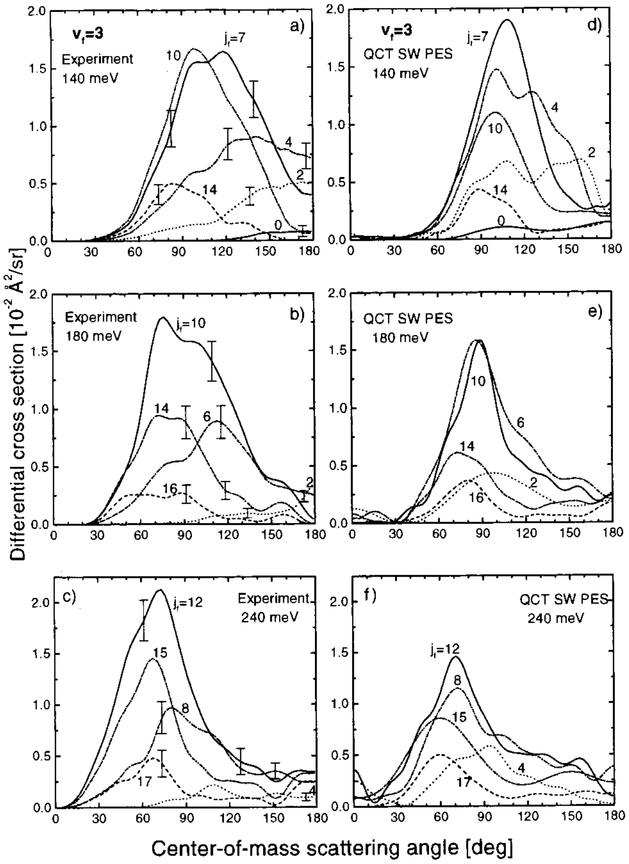

Figure 6. Same as Figure 5 but for the DF($v_f = 3$, j_f) product molecules.

The state specific reaction probabilities as a function of the total angular momentum *J* (opacity functions) were also calculated using the method of moments expansion in Legendre polynomials as described in ref 27.

IV. Results

A. Vibrationally State-Resolved Center-of-Mass Differential Cross Sections. The experimentally evaluated vibrationally state-resolved CM DCSs at 140, 180, and 240 meV collision energies are shown in Figures 4a−c. Their main features have been discussed in detail in refs 6, 8, and 25. Briefly, the observed general trends are the following: (i) At all three collision energies, the product CM angular distributions are predominantly backward, but significant scattering is also found in the forward region. (ii) The v_f state-resolved DCSs shift toward smaller CM scattering angles (from backward to forward scattering) as v_f increases. Appreciable scattering into $v_f = 0$ is only found at the two highest collision energies and is confined into the backward hemisphere. In contrast, the curves for $v_f = 1, 2, 3$, and 4 cover progressively a larger angular interval. (iii) The DCSs of all v_f shift as well toward smaller scattering angles with increasing collision energy.

The DCSs for $v_f = 4$, which were measured in the whole range of CM scattering angles at all three collision energies, are found to be quite flat except for scattering angles $\theta_{cm} <$ 20°, where a characteristic forward peak appears. The height

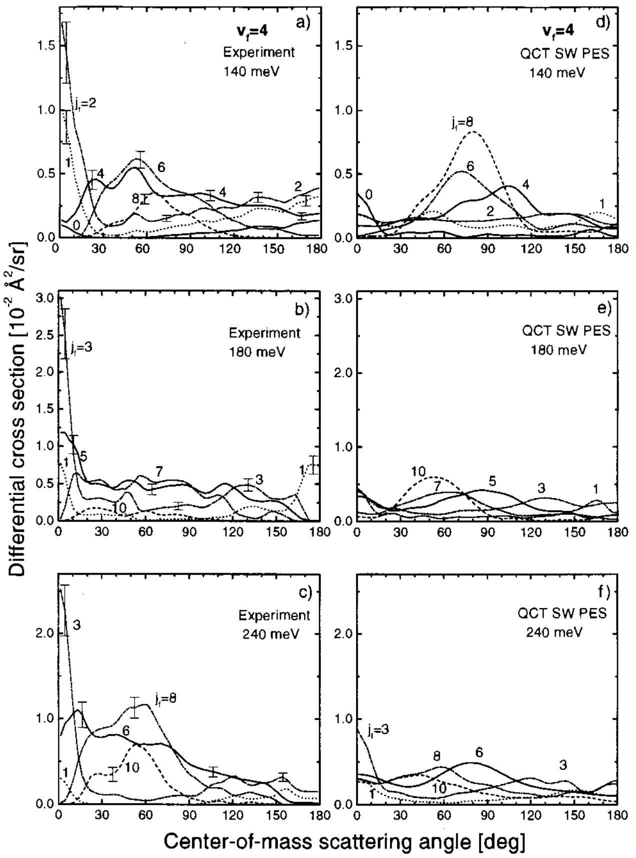

Figure 7. Same as Figure 5 but for the DF(v_f = 4, j_f) product molecules.

of this forward peak increases with collision energy and seems to level off at the highest collision energy measured.[8] The vibrational specificity of the $v_f = 4$ forward peak makes it interesting for the extraction of more detailed information on the rotational distribution of the forward scattered products (see section IV.B below). In addition, the $v_f = 4$ CM DCS displays a broad local maximum at about $\theta_{cm} \simeq 40°-70°$ at 240 meV collision energy, which is also present, but to a lesser extent, at the lower collision energies.

It should be noticed that the v_f state-resolved DCSs at 140 meV collision energy here presented (Figure 4a), differ slightly from those already published in ref 6. In this earlier preliminary report from our laboratory, an approximate analytical fitting method was employed for the evaluation of the CM DCSs, in which the translational energy width for each product state was calculated from a first-order Taylor expansion of the variance matrix.[5] Although that analytical approach is reliable for most scattering angles, it does not perform correctly for LAB angles where the CM Newton sphere of a given final product state is intersected close to its boundary (i.e, almost tangentially). This has a noticeable effect in the evaluation of the reactive yield into the CM forward and backward scattering regions, which is fully accounted for in the Monte Carlo convolution procedure employed in the present work (section II.B).

The QCT calculation on the SW PES reproduces reasonably well the main trends of the experimental v_f state-resolved DCSs at the three collision energies studied (see Figures 4d−f). In particular, a remarkably good agreement between theory and experiment is obtained for $v_f = 3$. For the rest of vibrational states, however, some noticeable discrepancies are observed. The QCT results clearly underestimate the $v_f = 1$ and $v_f = 2$ backward scattering at the three collision energies studied, the theoretical DCSs being shifted to sideways scattering angles with respect to the experimental ones. Interestingly, the experimentally deduced DCSs summed on v_f states show some undulations, especially at 180 and 240 meV collision energies, which reflect the maxima of the individual v_f state-resolved DCSs. On the contrary, the QCT total DCSs do not show such peak structure, the reason being the v_f-resolved DCSs take their maximum values at CM scattering angles that are closer together than in the experiment. As for $v_f = 4$, the QCT results reproduce qualitatively the experimental CM DCSs. The largest discrepancy occurs in the height of the forward peak, which is clearly underestimated in the classical calculation, and the amount of sideways scattering ($\theta_{cm} \approx 60-90°$), which is overestimated (in this case with the exception of 240 meV collision energy). At 240 meV collision energy, the QCT total forward peak is quite similar in height and width to the experimental one. However, whereas experimentally all the

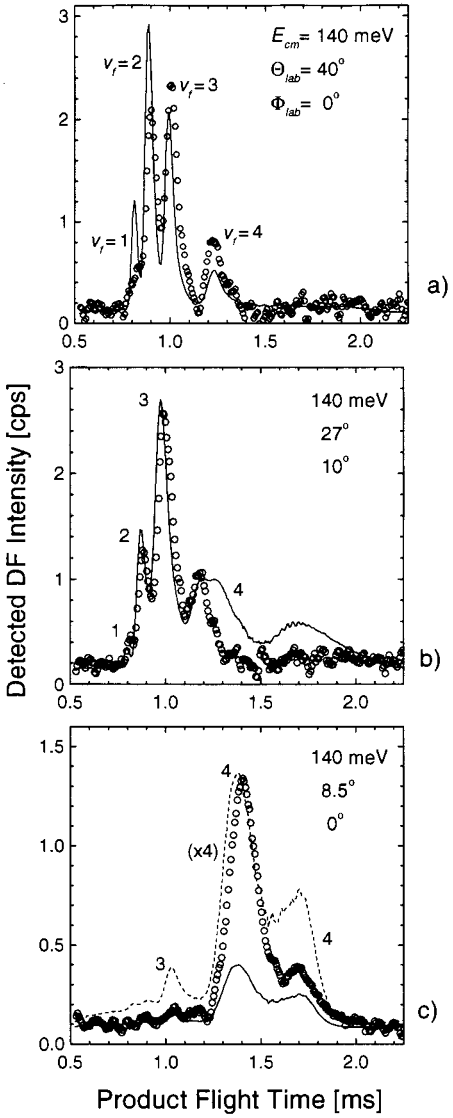

Figure 8. Comparison of experimental TOF measurements (open circles) and simulated spectra (lines) using the present QCT v_f, j_f DCSs for three representative sets of LAB scattering angles Θ_{lab}, Φ_{lab}, at 140 meV collision energy. Since the experimental cross sections are calibrated in absolute units, the QCT simulations do not include any adjustable parameter. The additional dotted line in panel (c) has been included for purposes of relative cross section comparisons and has been obtained by scaling the QCT simulated spectrum with the indicated factor of 4 in order to match the height of the $v_f = 4$ peak.

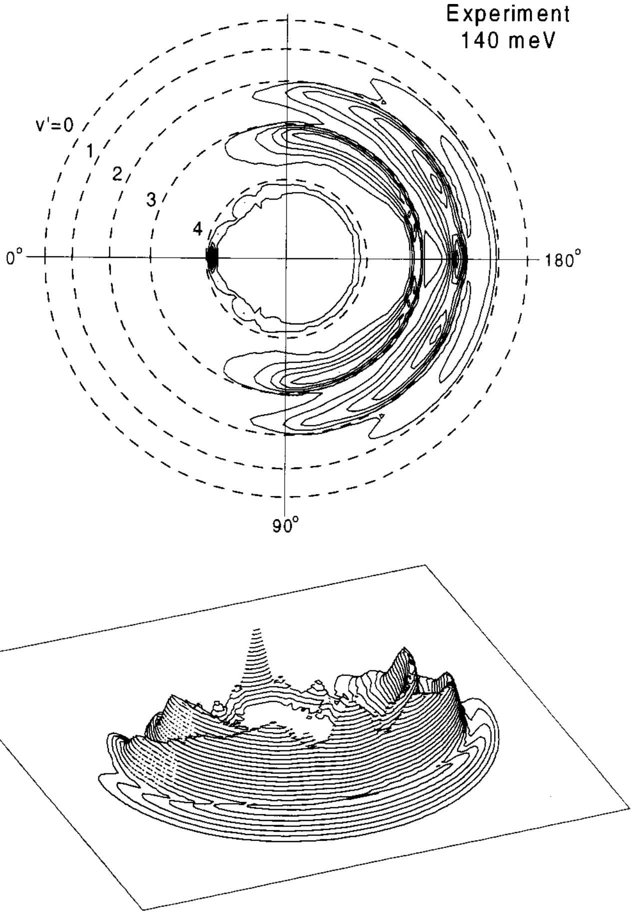

Figure 9. Center-of-mass scattering angle−recoil velocity contour map and 3D perspective for the DF products of the F + D_2 reaction at 140 meV obtained using the experimental v_f, j_f resolved DCSs. The dashed circles represent the maximum DF recoil velocity at each vibrational state.

forward scattering corresponds to $v_f = 4$, in the QCT case there is a substantial contribution from $v_f = 3$.

B. Rotationally State-Resolved Center-of-Mass Differential Cross Sections. Figures 5−7 display a representative set of the experimentally evaluated v_f, j_f state-resolved CM DCSs at the collision energies 140, 180, and 240 meV, respectively. The effect of increasing the collision energy on the v_f, j_f DCSs is two-fold: (i) an increase of the reaction cross section of the higher j_f states within each v_f state (i.e., an increase of the product rotational excitation); (ii) a global shift of each of the v_f, j_f DCSs toward smaller CM scattering angles. Interestingly, a similar backward−forward shifting can be observed at fixed collision energy as the product rotational quantum number j_f increases. Thus, the j_f-resolved DCSs shift to smaller scattering angles, both as the product rotational energy and as the collision energy increase. This resembles the behavior of the v_f state-resolved DCSs discussed in section IV.A (see Figure 4). Therefore, the DCSs for low j_f values tend to be confined into the backward region, whereas the DCSs for high j_f values have their maximum at smaller CM angles. In other words, the v_f products appear rotationally cooler at the large scattering angles (backward) than at the intermediate ones.

The j_f state-resolved DCSs for $v_f = 3$ shown in Figure 6 exemplify these observations. At 140 meV collision energy, for instance, the maximum in the j_f distribution for $v_f = 3$ shifts from $j_f \approx 4$ ($E_{rot} \approx 24$ meV) at $\theta_{cm} = 170°$ to $j_f \approx 10$ ($E_{rot} \approx 132.3$ meV) at $\theta_{cm} = 75°$. A similar effect is observed also at the two higher collision energies. For $v_f = 2$, the same behavior is observed (see Figure 5). For this vibrational state, as for $v_f = 3$, the maximum in the DCS of each j_f state shifts toward smaller angles with increasing j_f, moving from a backward-peaked distribution for $j_f = 0-5$, at all three collision energies, to a more sideways-peaked angular shape for the higher states $j_f \geq 10$. As for the $v_f = 1$ state (not shown), all j_f state-resolved DCSs are roughly confined into the backward hemisphere. The DCSs for $v_f = 1$, $j_f = 12-14$ are found to be the largest at all scattering angles at the three collision energies here considered, and no definite trend was observed in the overall form of the DCSs as j_f changes.

At this point, the specific rotational behavior observed for $v_f = 4$ requires a more detailed discussion. For this vibrational state, the above mentioned trends apply only for CM angles in the backward and sideways regions. For instance, the maximum cross section for backward scattering ($\theta_{cm} = 150°-180°$) corresponds to $j_f = 1-3$ and shifts to $j_f = 4-8$ for sideways scattering ($\theta_{cm} = 50°-120°$). However, in the narrow scattering angular region where the conspicuous forward peak appears ($\theta_{cm} < 20°$), the rotational distribution reaches its maximum for $j_f = 1-4$, depending on the collision energy of the experiment (see Figure 7). This is cooler by roughly 4 rotational quanta than at the sideways scattering angles. The cold j_f distribution found for the forward scattered $v_f = 4$ products is in contrast with the general trend observed with changing θ_{cm} for all final vibrational states, including $v_f = 4$, in the backward and sideways scattering region. Thus, the CM forward reactive scattering turns out to be a highly specific feature, not only vibrationally (it has been observed so far only for the DF($v_f = 4$) products[4,6,8,10,25]), but also rotationally. Only a small number of j_f states within $v_f = 4$ (typically three to four low rotational states ranging $j_f = 0-5$) account for most of the forward scattering at each collision energy.

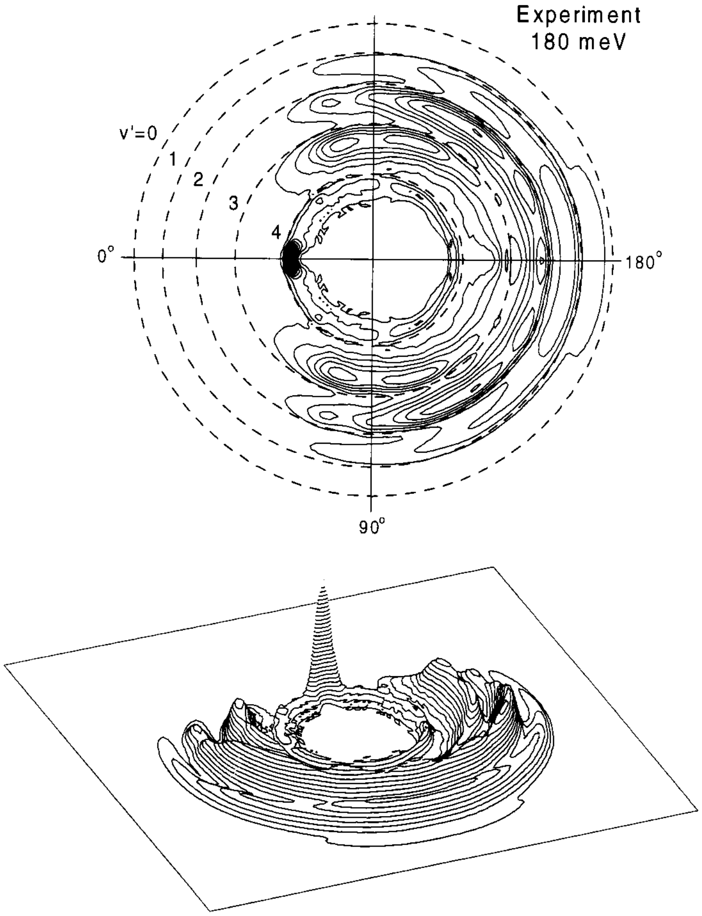

Figure 10. Same as Figure 9 but for the experiment at 180 meV collision energy.

The v_f, j_f DCSs calculated quasi--clasically on the SW PES for $v_f = 2$, 3, and 4 and $E_{cm} = 140$, 180, and 240 meV are represented in the right panels of Figures 5−7. Overall, the QCT results reproduce qualitatively the trends experimentally observed. In particular, the calculations predict backward scattered DF products with less rotational excitation than those sideways scattered, in good agreement with the observations. Furthermore, the QCT calculation agrees with the experiment in an overall increase of the DF rotational excitation for all final v_f states with increasing collision energy.

Significant discrepancies are, however, apparent between the experimental and QCT product rotational distributions. The QCT calculations predict j_f distributions for $v_f = 2$ and 3 which are significantly cooler than the experimental ones at all CM scattering angles. In the experiment at 140 meV collision energy, for instance, the product rotational states with the maximum reaction cross section at $\theta_{cm} \approx 140°$ are $j_f = 7{-}9$ for both $v_f = 2$ and $v_f = 3$. In contrast, the QCT calculation predicts $j_f = 4{-}5$ to be the most probable final rotational state at this scattering angle. The discrepancies are clearly appreciated when the comparison between experiment and theory is performed in the LAB frame. Figure 8 shows simulations based on the QCT v_f, j_f DCSs for three representative TOF spectra measured at 140 meV collision energy. The TOF spectra measured at $\Theta_{lab} = 40°$, $\Phi_{lab} = 0°$ (Figure 8a) and at $\Theta_{lab} = 27°$, $\Phi_{lab} = 10°$ (Figure 8b) correspond to DF($v_f = 1{-}4$) molecules scattered into backward and sideways CM scattering angles. The QCT simulations yield TOF peaks for $v_f = 1{-}3$ which are systematically faster (i.e., appear at shorter flight times) and narrower than the corresponding experimental peaks, which is an evidence for the cooler rotational distributions predicted by the calculation.

For $v_f = 4$, the QCT j_f distributions are rotationally hotter than the experimental ones over large intervals of CM angles in the sideways and early forward scattering region ($\theta_{cm} = 30°{-}120°$). The j_f value for which the maximum reaction cross section is obtained is larger in the QCT calculation than in the experiment by typically two or three quantum numbers. The largest differences with experiment are found for $\theta_{cm} = 40°{-}100°$ at 140 meV and for $\theta_{cm} = 30°{-}75°$ at 180 meV. The TOF spectrum shown in Figure 8b at $\Theta_{lab} = 27°$, $\Phi_{lab} = 10°$ and 140 meV collision energy, corresponds to an average CM scattering angle for DF($v_f = 4$) of $\theta_{cm} \approx 95° \pm 2°$. The QCT simulation predicts a much greater DF intensity than experimentally observed at the long flight times between 1.2−2.0 ms, which correspond to the arrival times of the high lying rovibrational states of $v_f = 4$, $j_f \geq 5$. This is a direct consequence of the hotter and broader rotational distribution obtained in the calculation for this vibrational state in comparison with the experimental one.

The QCT calculations reproduce well the state specificity of the forward scattering (i.e., the $v_f = 4$ DCS at $\theta_{cm} \approx 0°$ is dominated by scattering into low rotational states. As shown in Figure 7, the QCT j_f distribution for $v_f = 4$ at $\theta_{cm} = 0°{-}25°$, although somewhat cooler than the experimental one, is qualitatively correct at the three collision energies. The comparison in the LAB frame shown in Figure 8c for the 140 meV measurement at $\Theta_{lab} = 8.5°$, indicates a good agreement between theory and experiment for the location and shape (although not for the total intensity) of the $v_f = 4$ TOF peak, which is associated to small CM scattering angles, $\theta_{cm} \approx 0{-}15°$.

Finally, it is interesting to notice that in the QCT calculation the contribution of the high j_f states to the small-angle reactive scattering becomes progressively more relevant as the collision

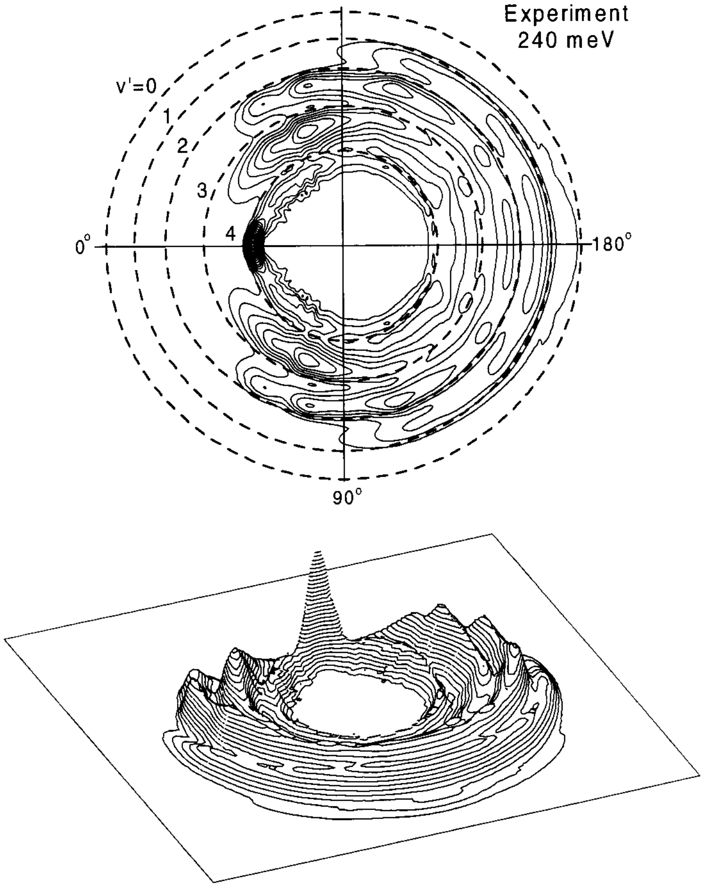

Figure 11. Same as Figure 9 but for the experiment at 240 meV collisio) energy.

energy increases. This effect, to a lesser extent, is also observed in the experiment. Hence, at 240 meV the QCT rotational distribution of the forward scattered $v_f = 4$ products is significantly broader than the experimental one, even though the rotational states with the largest cross section ($j_f = 3-4$) are well accounted for.

C. Center-of-Mass Angle−Velocity Polar Maps. Figures 9−11 display the CM velocity flux contour maps for the F + D_2 reaction at the three collision energies studied in this work. They were obtained from the experimental v_f, j_f DCSs following the method outlined in section II.B. The following trends can be recognized in the polar plots: (i) predominance of DF products into the backward scattering hemisphere for all vibrational states with the only exception of $v_f = 4$. (ii) Shift of the reactive flux toward the forward scattering hemisphere both as the internal energy of the products and/or the collision energy of the reactants increase. (iii) At large scattering (backward) angles, most of the reactive flux is found to be confined in a narrow interval of CM recoil velocities lying close to the maximum velocity kinematically allowed for each vibrational state. However, at smaller scattering angles the recoil velocity distribution becomes progressively broader and shifts toward smaller average values. This behavior is a consequence of the observed increase of the product rotational excitation in the sideways scattering region with respect to the backward one.

The most prominent feature of the polar maps at the three collision energies studied is the sharp maximum for $v_f = 4$ at $\theta_{cm} = 0°-15°$. In accord to the cold rotational distributions observed in the forward scattered DF($v_f = 4$), this peak is confined within a narrow interval of CM velocities close to the maximum recoil velocity for this vibrational state.

Figure 12 shows the CM velocity flux contour map obtained from the QCT v_f, j_f DCSs calculated on the SW PES at 240 meV collision energy. The more sideways character of the scattering into $v_f = 1$ and 2 and the smaller flux into forward scattering for $v_f = 4$ in comparison with the experimental one (Figure 11) can be appreciated in this map.

V. Discussion

The existence of a forward peak in the DCS of the highest accesible vibrational state of the products, HF($v_f = 3$) and DF($v_f = 4$), from the F + H_2 and F + D_2 reactions was first observed by Neumark and co-workers.[3,4] Since then its interpretation has been a challenge for subsequent experimental and theoretical investigations of this system. This feature was originally discussed as an evidence for a dynamical resonance.[3,4] However, this interpretation has been questioned since QCT calculations on different semiempirical and ab initio PESs have also succeeded in reproducing this forward peak.[16,17,29,30] The analysis of the forward scattering in both QCT and QM calculations indicated that it is associated with the largest accesible total angular momenta J that can yield reaction. Manolopoulos and co-workers[1,15] have interpreted their QM calculations as indicating that tunneling through the combined centrifugal and potential energy barrier was the sole reason for the enhancement of the forward scattering into HF($v_f = 3$) with respect to the QCT one. Similar conclusions were drawn from the analysis of time delays in the peaks of the cumulative reaction probability.[15] All the recent theoretical studies seem to rule out the original interpretation of the forward scattering as a manifestation of a pure reactive scattering resonance. The analysis of the present QCT calculations also shows unequivo-

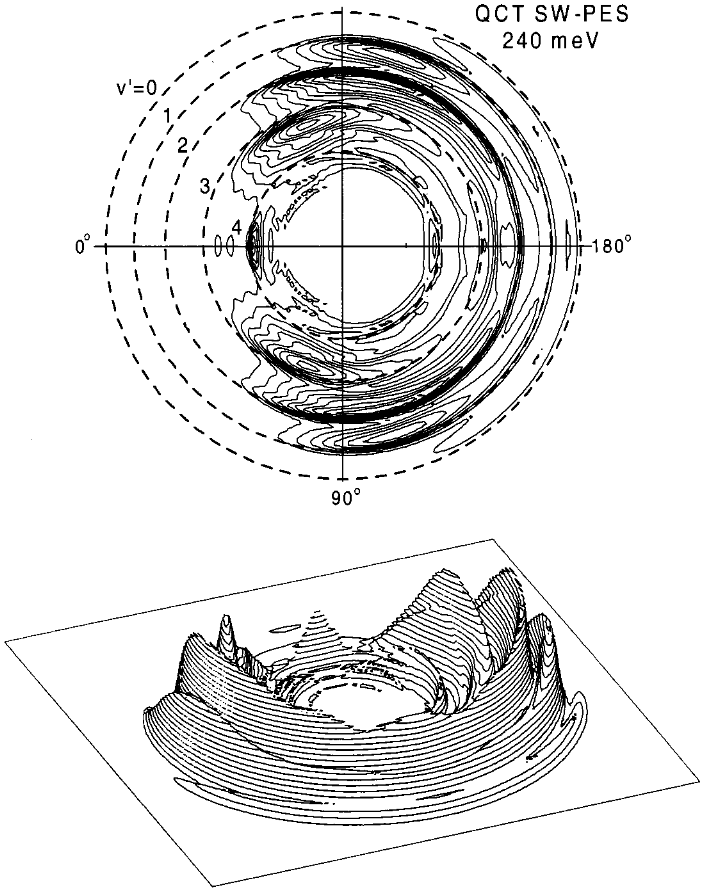

Figure 12. Same as Figure 9 but for the QCT calculation on the SW PES at 240 meV collision energy.

cally that the forward peak for the title reaction is exclusively caused by the largest accessible angular momenta (or impact parameters).

On intuitive grounds, if impulsive collisions dominate the reactive scattering, then backward scattering should be mainly due to collisions with small total angular momentum J (small impact parameters), whereas collisions with intermediate and large J values should lead to scattering into the sideways and forward regions. Also, small values of J will favor the production of DF products into low j_f states within each v_f, and conversely, the highest j_f states will be produced in collisions with large values of J. This would explain the trends observed in the experimental v_f, j_f DCSs discussed in section IV.B.

In order to check this model further, the QCT v_f, j_f reaction probabilities as a function of J, $P(J\ ;v_f, j_f)$ (opacity functions) have been calculated for the F + $D_2(v_i = 0, j_i = 0)$ reaction on the SW PES at 140 meV collision energy, and are shown in Figure 13 for the $v_f = 2$, 3, and 4 states. As can be seen, there is a shift of the maximum of the opacity functions toward larger values of J with increasing j_f for the three v_f states. For $v_f = 2$, for instance, the largest reaction probability for $j_f = 2$ occurs at $J \leq 5$, whereas for $j_f = 16$ it becomes largest at $J = 17-20$. As a consequence, the QCT CM DCS for $v_f = 2$, $j_f = 2$ peaks at backward angles ($\theta_{cm} \approx 165°$), whereas for $v_f = 2$, $j_f = 16$ it peaks at sideways angles ($\theta_{cm} \approx 90°$), which is in qualitative agreement with the experiment (see Figure 5). Similar considerations apply to the higher product vibrational states. For $v_f = 3$, the most probable rotational states at 140 meV, both in the experiment and in the QCT calculation, are $j_f = 7-10$ (see Figure 6). As can be seen in Figure 13b, the large value of the reaction probability for $J = 12-18$ is responsible for the large maximum at sideways scattering angles observed in the CM DCSs for these rovibrational states. Furthermore, the prominent sideways scattering observed for the states $v_f = 4$, $j_f = 6-8$ (Figure 7) can be rationalized in the same way. In this case, it is related to the efficient reaction of F$-$$D_2$ collisions with angular momenta $J = 14-20$ (Figure 13c). One direct consequence is that the hotter rotational distributions predicted by the QCT calculation as compared with the experimental ones for DF products in $v_f = 4$ at CM angles 30°$-$100° (see Figures 8a and d) must be related with the overestimation of the reaction probability for states with $j_f \geq 5$ at large J values. In fact, this is the case for the F + H_2 isotopic variant of the reaction for which both QM and QCT calculations are available on the SW PES. The QCT $P(J)$ for the highest vibrational state ($v_f = 3$ for F + H_2) show a pronounced maximum for intermediate J values, which is much smaller in the QM $P(J)$. As a result the QCT calculations predict substantially more sideways scattering into that state than that found in the QM DCSs, which, consequently, are also rotationally cooler.

The QCT opacity functions presented in Figure 13 can also be used to explain the specific behavior of the forward scattered DF($v_f = 4$, j_f) molecules, which, as discussed above, are mostly in low rotational states. Figure 13c shows that for $v_f = 4$ the classical $P(J)$ for small j_f extends from low to high values of J, in some cases with a double maximum structure (e.g., the $P(J)$ curve for $j_f = 1$). The high J values contribute to forward scattering, whereas the small J values give rise to backward scattering. Interestingly, the QCT calculation at 140 meV shows that for larger j_f values, collisions with high J yield preferentially sideways scattering with little contribution to the forward peak. Hence, it turns out that in order for a DF($v_f = 4$) product molecule to be scattered in the forward direction, it must be

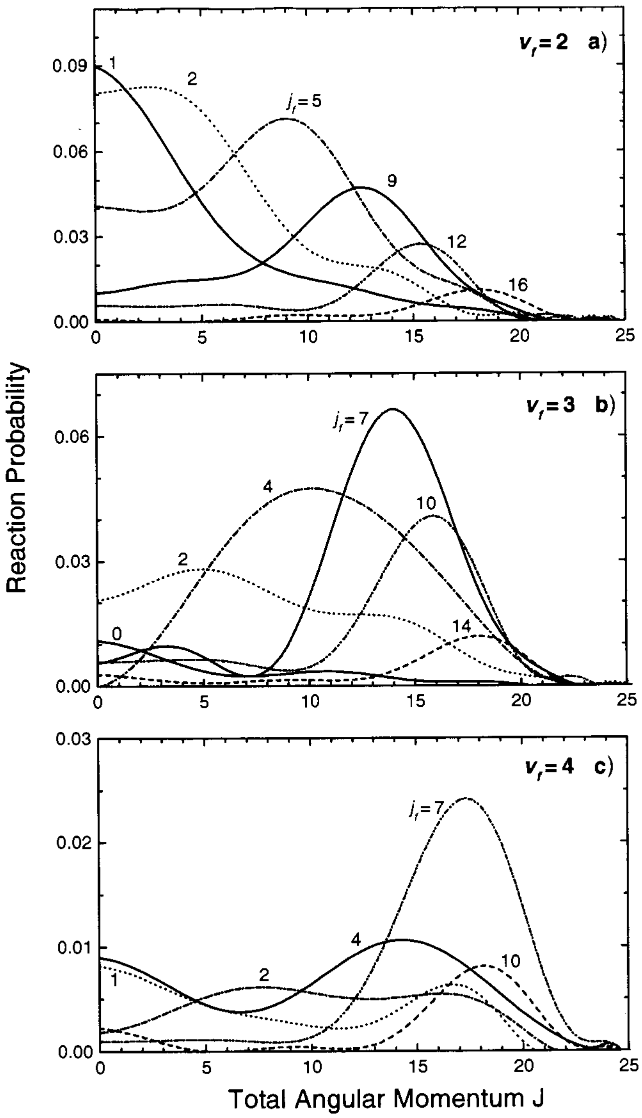

Figure 13. QCT F + D_2 ($j_i = 0$) reaction probabilities at 140 meV collision energy as a function of the total angular momentum *J* (opacity functions) for DF product molecules in representative rovibrational states: (a) $v_f = 2$, j_f ; (b) $v_f = 3$, j_f ; (c) $v_f = 4$, j_f.

produced in reactive collisions with high orbital angular momentum and also be in a low final j_f state.

VI. Conclusions

In this work, product rotational state-resolved differential cross sections (DCS) have been evaluated from high resolution crossed molecular beam experiments on the F + D_2 reaction at the collision energies of 140, 180, and 240 meV. These results have been compared with quasiclassical trajectory (QCT) calculations on the ab initio potential energy surface (PES) by Stark and Werner (SW).

The most significant trends of the experimentally evaluated v_f, j_f state resolved DCSs are (i) The CM DCSs of the j_f rotational states within a given vibrational state v_f shift from the backward to the sideways and forward scattering regions with increasing quantum number j_f. Thus, the scattering into the low rotational states is found to be confined at the large CM scattering angles, whereas the DCS of the more excited j_f states covers a progressively broader angular interval and peaks at intermediate angles. (ii) The only exception to this trend is found for the forward scattered DF products in $v_f = 4$. The CM DCS for this vibrational state presents a narrow maximum associated exclusively with low rotational states. The DF molecules scattered into $v_f = 4$ at CM angles close to $\theta_{cm} = 0°$ are rotationally colder (typically 3−5 rotational quanta) than those scattered at intermediate angles.

These trends are, in general, well reproduced by the QCT calculations. However, this comparison must be taken with care since, although in some instances there is a reasonable good agreement between QCT and QM state-resolved DCSs calculated on the same PES,[23,27,31] a rigorous interpretation of the dynamics of a reactive system must be based on exact QM calculations. Moreover, the proper assessment of the potential energy surface can only be achieved by a direct simulation of the high resolution experimental results using accurate QM state-resolved DCSs.[11,14,19,32]

One of the most important conclusions of the present study has been the experimental confirmation that the F + D_2 forward scattering is not only vibrationally specific but also rotationally, and, moreover, the finding that the forward peak is built with the contribution of a few low rotational states only (i.e., it is rotationally cold. The analysis based on the QCT calculations for the system corroborates previous QM studies for the F + H_2 reaction in showing that this behavior can be rationalized by resorting to the reaction probability as a function of the total angular momentum and indicate that for molecules scattered into the forward region, there is an inefficient transfer of orbital to rotational angular momentum, and the orbital angular momentum remains roughly unchanged.

Acknowledgment. B. Martínez-Haya acknowledges finantial support from the Human Capital and Mobility Programme of the European Union and from the Programme “Acciones para la Incorporación de Doctores y Tecnólogos” of the Ministry of Education and Culture of Spain. The work of L. Y. Rusin in Göttingen was financed by the Deutsche Forschungsgemeinschaft. F. J. Aoiz and L. Bañares acknowledge funding from the DGICYT of Spain (Grant PB95-0918-C02).

References and Notes

(1) Manolopoulos, D. E. *J. Chem. Soc., Faraday Trans.* **1997**, *93*, 673 and references therein.

(2) Anderson, J. B. *Adv. Chem. Phys.* **1980**, *41*, 229 and references therein.

(3) Neumark, D. M.; Wodtke, A. M.; Robinson, G. N.; Hayden, C. C.; Lee, Y. T. *J. Chem. Phys.* **1985**, *82*, 3045.

(4) Neumark, D. M.; Wodtke, A. M.; Robinson, G. N.; Hayden, C. C.; Shobatake, R.; Sparks, R. K.; Schafer, T. P.; Lee, Y. T. *J. Chem. Phys.* **1985**, *82*, 3067.

(5) Faubel, M.; Rusin, L. Y.; Sondermann, F.; Schlemmer, S.; Tappe, U.; Toennies, J. P. *J. Chem. Phys.* **1994**, *101*, 2106.

(6) Faubel, M.; Martínez-Haya, B.; Rusin, L. Y.; Tappe, U.; Toennies, J. P. *Chem. Phys. Lett.* **1995**, *232*, 197.

(7) Faubel, M.; Martínez-Haya, B.; Rusin, L. Y.; Tappe, U.; Toennies, J. P. *Z. Phys. Chem.* **1995**, *188*, 197.

(8) Faubel, M.; Martínez-Haya, B.; Rusin, L. Y.; Tappe, U.; Toennies, J. P.; Aoiz, F. J.; Bañares, L. *Chem. Phys.* **1996**, *207*, 227.

(9) Baer, M.; Faubel, M.; Martínez-Haya, B.; Rusin, L. Y.; Tappe, U.; Toennies, J. P.; Stark, K.; Werner, H.-J. *J. Chem. Phys.* **1996**, *104*, 2743.

(10) Faubel, M.; Martínez-Haya, B.; Rusin, L. Y.; Tappe, U.; Toennies, J. P. *J. Phys. Chem. A* **1997**, *101*, 6415.

(11) Baer, M.; Faubel, M.; Martínez-Haya, B.; Rusin, L. Y.; Tappe, U.; Toennies, J. P. *J. Chem. Phys.* **1998**, *108*, 9694.

(12) Ayabakan, M.; Faubel, M.; Martínez-Haya, B.; Rusin, L. Y.; Sevryuk, M. B.; Tappe, U.; Toennies, J. P. *Chem. Phys.* **1998**, *229*, 21 and references therein.

(13) Stark, K.; Werner, H.-J. *J. Chem. Phys.* **1996**, *104*, 6515.

(14) Aoiz, F. J.; Bañares, Martínez-Haya, B.; L.; Manolopoulos, D. E.; Castillo, J. F.; Stark, K.; Werner, H.-J. *J. Phys. Chem. A* **1997**, *101*, 6403.

(15) Castillo, J. F.; Manolopoulos, D. E.; Stark, S.; Werner, H.-J. *J. Chem. Phys.* **1996**, *104*, 6531.

(16) Aoiz, F. J.; Bañares, L.; Herrero, V. J.; Sáez Rábanos, V.; Stark, K.; Werner, H. J. *Chem. Phys. Lett.* **1994**, *223*, 215.

(17) Aoiz, F. J.; Bañares, L.; Herrero, V. J.; Sáez Rábanos, V.; Stark, K.; Werner, H.-J. *J. Phys. Chem.* **1994**, *98*, 10665.

(18) Aoiz, F. J.; Bañares, L.; Faubel, M.; Martínez-Haya, B.; Rusin, L. Y.; Tappe, U.; Toennies, J. P. *Chem. Phys.* **1996**, *207*, 245.

(19) Honvault, P.; Launay, J. M. *Chem. Phys. Lett.* **1998**, *287*, 270.

(20) Chapman, W. B.; Blackmon, B. W.; Nesbitt, D. J. *J. Chem. Phys.* **1997**, *107*, 8193.

(21) Dharmasena, G.; Phillips, T. R.; Shokhirev, K. N.; Parker, G. A.; Keil, M. *J. Chem. Phys.* **1997**, *106*, 9950.

(22) Dharmasena, G.; Copeland, K.; Young, J. H.; Lasell, R. A.; Phillips, T. R.; Parker, G. A.; Keil, M. *J. Phys. Chem. A* **1997**, *101*, 6429.

(23) Castillo, J. F.; Hartke, B.; Werner, H.-J.; Aoiz, F. J.; Bañares, L.; Martínez-Haya, B. *J. Chem. Phys.* **1998**, in press.

(24) Faubel, M.; Martínez-Haya, B.; Rusin, L. Y.; Tappe, U.; Toennies, J. P. *J. Phys. D: Appl. Phys.* **1996**, *29*, 1885.

(25) Martínez-Haya, B., Ph.D. Thesis, Universidad Complutense Madrid, June 1996, Max-Planck-Institut für Strömungsforschung: Göttingen, 1996 (Bericht 101/1996, (ISSN-0436-1199).

(26) Buck, U.; Meyer, H.; LeRoy, R. J. *J. Chem. Phys.* **1984**, *80*, 5589.

(27) Aoiz, F. J.; Herrero, V. J.; Sáez Rábanos, V. *J. Chem. Phys.* **1992**, *97*, 7423.

(28) Aoiz, F. J.; Bañares, L.; Herrero, V. J.; Sáez Rábanos, V.; Stark, K.; Werner, H.-J. *J. Chem. Phys.* **1995**, *102*, 9248.

(29) Takayanagi, T.; Sato, S. *Chem. Phys. Lett.* **1988**, *144*, 191.

(30) Aoiz, F. J.; Bañares, L.; Herrero, V. J.; Sáez Rábanos, V. *Chem. Phys.* **1994**, *187*, 227.

(31) Schnieder, L.; Seekamp-Rahn, K.; Wrede, E.; Welge, K. H. *J. Chem. Phys.* **1997**, *107*, 6175.

(32) Bañares, L.; Aoiz, F. J.; Herrero, V. J.; D'Mello, M. J.; Niederjohann, B.; Seekamp-Rahn, K.; Wrede, E.; Schnieder, L. *J. Chem. Phys.* **1998**, *108*, 6160.